NO EVIDENCE FOR IRIS

BY DENNIS L. HARTMANN AND MARC L. MICHELSEN

Careful analysis of data reveals *no* shrinkage of tropical cloud anvil area with increasing SST

Lindzen et al. (2001, hereafter LCH) present observational analysis suggesting that the area coverage of anvil clouds associated with tropical convection is less extensive when sea surface temperatures (SSTs) are higher. This conclusion is based on a negative correlation between the fractional area coverage by high clouds and the average SST under the clouds. LCH observe this correlation in about 20 months of Geostationary Meteorological Satellite (GMS) radiance data for the oceanic regions in the domain between 30°S–30°N and 130°E–170°W. LCH then used this correlation to hypothesize that increased SST leads to reduced area of anvil cloud associated with convective cores in the Tropics. They then concluded that reduced anvil cloud would give rise to a negative feedback through reduced upper-tropospheric water vapor and diminished greenhouse effect.

We have obtained the cloud data from LCH and have investigated the geographical patterns of cloud fraction variation that are associated with variations in the cloud-weighted SST. These patterns show that the changes in cloud-weighted SST for clouds with emission temperatures less than 260 K are dominated by cloud variations in subtropical latitudes. These variations are geographically separated from the variations in the deepest convective clouds (those with emission temperatures less than 220 K), which occur only near the equator where surface temperatures are highest. LCH assume that the coldest clouds are representative of the convective cores that feed anvil clouds. In this article we show that the deep convective cores are separated by more than 1000 km from the clouds that are associated with most of the variation in cloud-weighted SST. The explanation for the correspondence between cloud-weighted SST and cloud area is thus a shift in the latitude or longitude of the cloudiness and not a change in the relation between deep convective and associated tropical anvil cloud amounts. These latitude and longitude shifts are associated with meteorological forcing and not with SST forcing. Much of the meteorological forcing seems to originate in the extratropics and is probably unrelated to tropical SSTs. *If the SSTs and the near-equatorial clouds remain fixed and constant, any variation in subtropical cloud fraction will produce the negative correlation on which LCH base their negative feedback hypothesis.*

AFFILIATION: HARTMANN AND MICHELSEN—Department of Atmospheric Sciences, University of Washington, Seattle, Washington
CORRESPONDING AUTHOR: Dennis L. Hartmann, Department of Atmospheric Sciences, University of Washington, 710 Atmospheric Sciences/Geophysics Building, Box 351640, Seattle, WA 98915-1640
E-mail: dennis@atmos.washington.edu

In final form 25 May 2001

DATA AND ANALYSIS PROCEDURES. The 11-μm GMS radiance data used in LCH (provided by M.-D. Chou) consisted of daily fractional cloud amounts binned by emission temperature for clouds with 11-μm emission temperatures lower than 210 K and between the temperatures of 210, 220, 230, 240, 250, 260, 270, and 310 K. Daily means are given in the domain from 40°S to 40°N and 90°E to 170°W at 1° × 1° latitude–longitude resolution for the period from 1 January 1998 to 31 August 2000. We then developed a cumulative cloud dataset that gives the fraction of each box with 11-μm emission temperatures less than 210, 220, 230, 240, 250, 260,

270, and 310 K. Henceforth we will denote clouds with 11-μm emission temperatures less than 260 K with the notation $T_{11} < 260$ K and those with temperatures less than 220 K as $T_{11} < 220$ K. The Reynolds SST data were obtained from the National Oceanic and Atmospheric Administration–Cooperative Institute for Research in Environmental Sciences (NOAA–CIRES) Climate Diagnostics Center (data available online at http://www.cdc.noaa.gov/), and interpolated from weekly to daily values. In order to calculate the cloud-weighted SST and the cloud area over the ocean, a land mask is required. We used the land mask that is associated with the Reynolds SST data.

With these data we use the formulas in LCH to calculate the cloud fraction and cloud-weighted SST over the domain used by LCH, the ocean areas in the region between 30°S–30°N and 130°E–170°W. The cloud-weighted SST, $\overline{T}$, is the product of cloud cover and SST, weighted by area and summed over all the 1° × 1° grid boxes in the region of interest. The cloud fraction, $\overline{A}$, is the cloud fraction A_n averaged over the area of all the 1° × 1° boxes in the region of interest weighted by area, which is incorporated as the cosine of latitude, $\cos\theta_n$. The formulas used here are reproduced from LCH, below:

$$\overline{A} = \frac{\sum_n A_n \cos\theta_n}{\sum_n A_n \cos\theta_n} \qquad \overline{T} = \frac{\sum_n A_n T_n \cos\theta_n}{\sum_n A_n \cos\theta_n} . \quad (1)$$

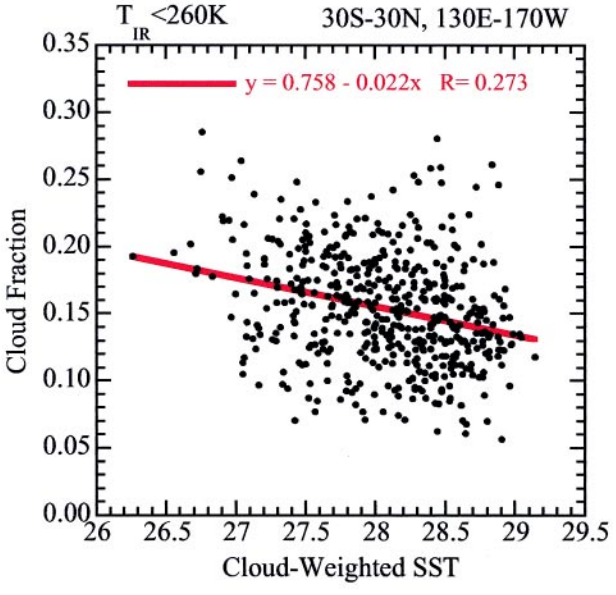

FIG. 1. Scatter diagram of $T_{11} < 260$ K cloud area fraction vs the cloud-weighted SST for the ocean areas in the region 30°S–30°N and 130°E–170°W. Also shown is the linear regression of cloud fraction on cloud-weighted SST.

In both cases, only ocean areas are included in the averages. Increases in the cloud-weighted SST arise primarily from cloud fraction decreasing over colder ocean areas and/or increasing over higher SST regions. We plot the scatter diagram of daily values of fraction covered by clouds with tops colder than 260 K versus the cloud-weighted SST for all the days in the dataset in Fig. 1. The scatter diagram and the resulting linear regression slope we obtain are very similar to those shown in Fig. 5a of LCH. Although the regression line is very similar, our scatter diagram is not identical to that of LCH. We think this may be because of differences in the land mask that was used.

Because the daily values of cloud fraction and cloud-weighted SST have low-frequency variations, we have done the analysis with and without high-pass filtering of the time series of area-average cloud cover and cloud-weighted SST. We use a 61-day running-mean smoother, including only days when data are available to compute the low-pass-filtered time series, and then subtract it from the original time series to obtain the high-pass-filtered data. In agreement with the results of LCH, removing the low-frequency variation does not change the basic conclusions. Thus we perform the analysis described in LCH, and obtain a very similar negative correlation between cloud-weighted SST and cloud fraction.

SPATIAL SIGNATURE OF CLOUD-WEIGHTED SST. We now ask whether the variations in cloud-weighted SST are associated with particular geographical patterns of cloud coverage. We have done this in two ways that yield very similar results. Using the scatter diagram in Fig. 1 as a basis, we have averaged the days on which the cloud-weighted SST was less than average and the cloud coverage was more than average, and compared that map with the average for the days when the cloud-weighted SST was greater than average and the cloud cover was less than average. This should capture any spatial patterns associated with the slope in Fig. 1.

We have also done a linear regression between the time series of cloud-weighted SST and the map of cloud fraction. The times series of daily cloud fraction for each 1° × 1° grid box is regressed on the time series of cloud-weighted SST calculated for the 30°S–30°N, 130°E–170°W domain. Formally, the regression is a least squares fit of the cloud data to the cloud-weighted SST of the following form:

$$A_n(t) = a_n \overline{T}(t) + b_n , \quad (2)$$

where the subscript n indicates one of the 1° × 1° grid boxes and t is time. Before the regression is performed, the time series of $\overline{T}$ is divided by its standard deviation so that a_n is a dimensionless number indicating the fractional change in cloud area that is linearly related to a one standard deviation change in $\overline{T}$. The change in cloud fraction when the cloud-weighted SST goes from –1 to +1 standard deviation is twice the value in the map.

The map of the regression coefficient a_n is shown in Fig. 2 for the case of clouds with emission temperatures less than 260 K. Also shown in Fig. 2 are the 200-mb wind vectors from the European Centre for Medium-Range Weather Forecasts analysis product, regressed onto the cloud-weighted SST in the same manner as the cloud fraction. In Fig. 2 the entire domain for which the cloud data are available is shown, although the cloud-weighted SST is calculated only for the ocean areas in the smaller domain between 30°S–30°N and 130°E–170°W. The cloud-weighted SST was high-pass filtered prior to the regression to remove seasonal and longer timescales, but regression maps are very similar when calculated with the unfiltered data.

Figure 2 shows that the largest cloud fraction changes associated with variations in the cloud-weighted SST occur in the subtropics, where the SST is reduced, and not over the warmer waters nearer to the equator, which we normally associate with tropical deep convection. Increases (decreases) in cloud-weighted SST are associated with decreased (increased) cloudiness in the subtropics, concentrated between 20°–30°S and 20°–30°N. Cloudiness changes of opposite sign occur in the band from 10°S to the equator, which is the region of highest SST and most intense deep convection in this region. Near 25°S in the Pacific east of Australia cloud fraction variations are very large in comparison to the average cloud fraction and are strongly correlated with wind anomalies that are suggestive of Rossby wave trains propagating into the region from the extratropics (Hoskins and Karoly 1981). Near 25°N cloudiness variations are associated with variations in the strength of the midlatitude westerly jet stream. Zonal wind variations in the Northern Hemisphere and Rossby waves in the Southern Hemisphere are probably not related to each other, but each separately influences the cloud-weighted SST. The maximum wind anomalies associated with a 1 standard deviation increase in cloud-weighted SST are of order 10 m s^{-1} at 200 mb, which is a substantial anomaly. The wind anomalies at 850 mb (Fig. 3) are consistent with those shown at 200 mb (Fig. 2).

We have also regressed the amount of cloud with tops colder than 220 K onto the cloud-weighted SST

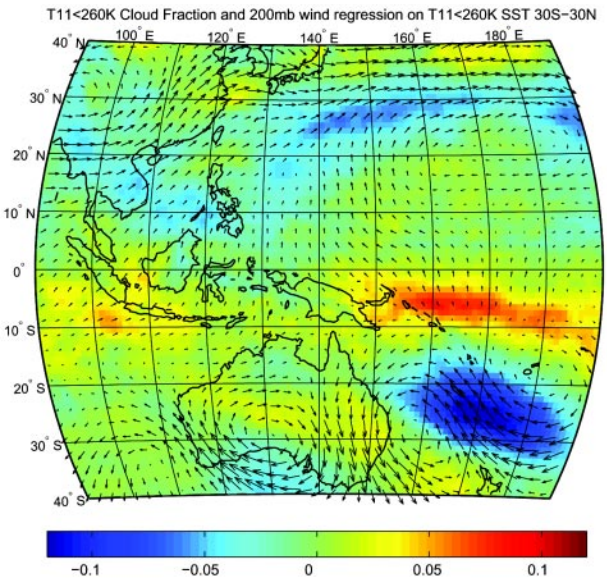

FIG. 2. Regression of the T_{11} < 260 K cloud cover and the 200-mb wind vectors onto the T_{11} < 260 K cloud-weighted SST for the region 30°S–30°N, 130°E–170°W. The cloud-weighted SST was high-pass filtered prior to the regression. The largest wind vectors shown have magnitude of about 10 m s^{-1}. The map projection is a Hammer equal-area projection.

under clouds with tops colder than 260 K. This will show how the changes in the coldest, deepest clouds vary with the T_{11} < 260 K cloud-weighted SST. This regression map is shown in Fig. 3, along with the regression of the 850-mb winds onto the SST weighted for clouds with T_{11} < 260 K. Near the equator the coldest clouds show a pattern similar to the T_{11} < 260 K clouds, because the coldest clouds and warmer convective clouds appear as part of the same cloud systems there. In the subtropics, where most of the signal in cloud-weighted SST is generated, there is little variation in the coldest cloud, despite the large dynamical forcing supplied by the wind variations. This may be because lower SSTs south of 20°S and north of 10°N cannot support really deep convection, and so optically thick clouds with tops colder than 220 K are extremely rare at these higher latitudes and lower SSTs.

Figure 4 shows the average T_{11} < 260 K and T_{11} < 220 K cloud fractions zonally averaged for ocean areas in the LCH longitude domain of 130°E–170°W. The ratio of the area coverage by T_{11} < 220 K to T_{11} < 260 K is 0.2 between 15°S and 15°N, but outside this near-equatorial belt the amount of the coldest clouds decreases rapidly, while the warmer cloud fraction may even increase. This is again because the T_{11} < 220 K clouds are only common over the highest SSTs and become extremely rare in the subtropics.

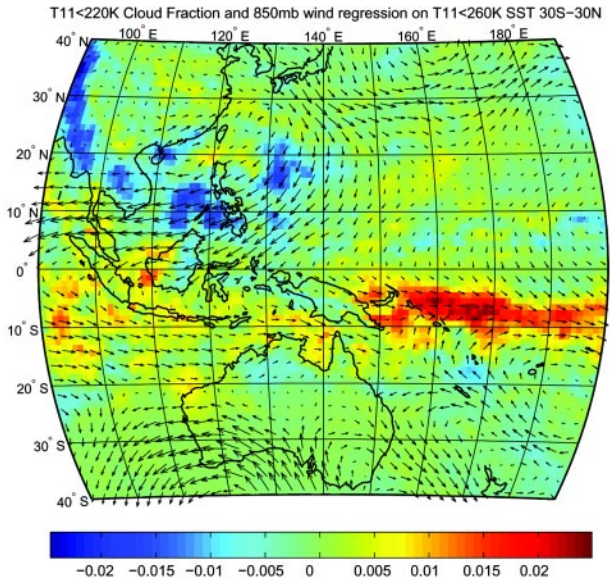

FIG. 3. Regression of the T_{11} < 220 K cloud cover and the 850-mb wind vectors onto the T_{11} < 260 K cloud-weighted SST for the region 30°S–30°N, 130°E–170°W as in Fig. 2. The largest wind vectors shown have a magnitude of about 5 m s^{-1}.

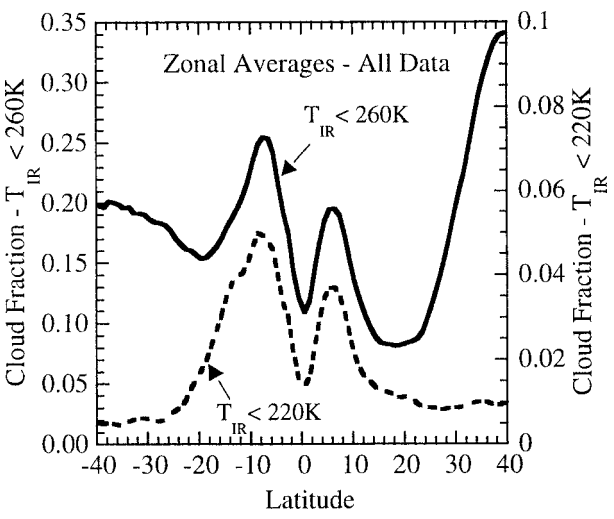

FIG. 4. Zonally averaged T_{11} < 260 K cloud fractions for the oceanic areas in the region 130°E–170°W for all days with data in the period 1 Jan 1998–31 Aug 1999.

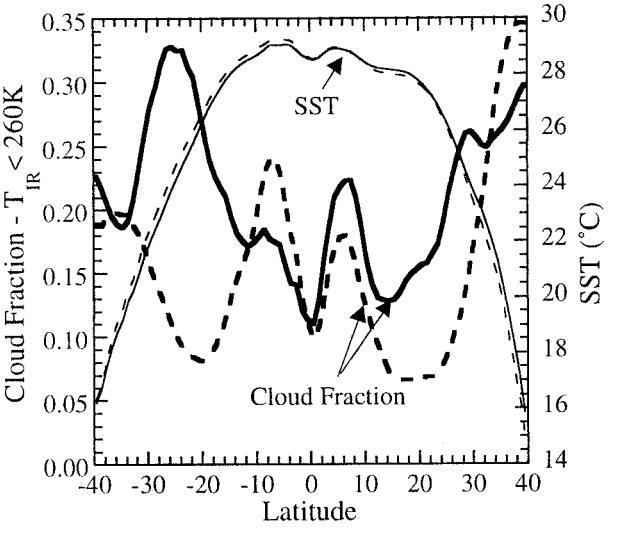

FIG. 5. Zonally averaged T_{11} < 260 K cloud fraction and SST composites for days when cloud-weighted SST is less than average and cloud fraction is greater than average (solid lines) and days when cloud-weighted SST is greater than average and cloud fraction is less than average (dashed lines) in the region 30°S–30°N, 130°E–170°W based on the unfiltered data in Fig. 1.

Thus the subtropical clouds that provide most of the variation in cloud-weighted SST and most of the negative correlation with mean cloud cover are not physically connected to deep tropical convective cores and, in fact, are separated from them by about 1000 km.

Figure 5 shows zonal averages of the cloud cover and SST for the composites obtained from averaging just days when the cloud-weighted SST was greater than average and the cloud fraction was less than average and comparing this with the averages for the days when the cloud-weighted SST was less than average and the cloud fraction was greater than average. The averages are only for the ocean areas within the box used by LCH, which extends between 30°S–30°N and 130°E–170°W. The two composites of SST are virtually identical, so the differences in SST are not significant. Decreases (increases) in cloud-weighted SST result primarily from increases (decreases) of cloud fraction in the subtropics, where SST is lower. Near the equator cloudiness shifts from 8°S to 8°N, but the change in average cloud cover in the band from 15°S to 15°N is quite small. Both the change in cloud-weighted SST and the change in cloud coverage arise primarily from the subtropics in both hemispheres at latitudes greater than 15°. *Again, since the changes in cloud cover occur in latitudes where deep convective cores do not occur, it is unreasonable to associate the negative slope in Fig. 1 with a change in the ratio of anvil area to convective core area.* By comparing the SST in Fig. 5 with the cloud fractions in Fig. 4, one can see that the climatological abundances of both convective and anvil clouds increase with increasing SST. Small variations in zonal mean SST near the equator correlate positively with substantial variations in zonal mean cloud cover. Comparing 8°N and 8°S suggests strong positive sensitivity of convective and anvil cloud amounts to SST. It would be dangerous to apply this correlation naively to climate sensitivity analysis, however.

If one still believes that the cloud-weighted SST is a useful statistic, one can try to avoid the problem of mixing subtropical and tropical clouds in the same analysis by constraining the domain of interest to lower latitudes, but this does not lend any support to the LCH hypothesis. When the domain of interest is limited to regions nearer the equator, a negative correlation between cloud-weighted SST and cloud fraction is still produced by any variation in cloud fraction over the colder regions. In this case both the $T_{11} < 220$ K and the $T_{11} < 260$ K cloud fractions show negative correlations with cloud-weighted SST. Table 1 shows the results of regressions between daily cloud amount and cloud-weighted SST in the LCH zonal domain for different choices of latitudinal domain, for both the raw time series of cloud-weighted SST and cloud fraction and for the time series with the low-pass-filtered time variations removed. The correlation magnitude necessary to reject a null hypothesis of zero correlation at the 95% confidence level is about 0.09 for these datasets. This is based on estimating the degrees of freedom using the formula of Leith (1973). With such a low correlation, however, the slope is quite uncertain and could be very close to zero. For a correlation of 0.1, only 1% of the variance is explained by the linear fit. As the latitudinal domain is reduced from 30°S–30°N to 15°S–15°N, the standard deviation of cloud-weighted SST decreases from about 0.5 to about 0.25 for $T_{11} < 260$ K clouds, because the low SSTs in the subtropics are no longer within the domain. Negative correlations between cloud-weighted SST and cloud coverage persist as the boundaries of the domain are constrained to lower latitudes, although the statistical significance of the slopes decreases. For the domains constrained nearer the equator, however, the slopes of the $T_{11} < 220$ K regression lines are also significantly negative. This means that the amount of convection as measured by the $T_{11} < 220$ K fraction varies in proportion to the anvil cloud, as measured by $T_{11} < 260$ K, and vice versa. The slopes are now simply measuring the tendency of all cloud types associated with deep tropical convection near the equator to vary together, as discussed in relation to Figs. 4 and 5, and do not indicate a reduction of cloud anvil area with increased SST. Note that the $T_{11} < 220$ K cloud area is only about 20% of the $T_{11} < 260$ K cloud area, so one must multiply the $T_{11} < 220$ K slopes by a factor of 5 before comparing them with the $T_{11} < 260$ K slopes. When this is done the slopes are comparable in magnitude, indicating that when normalized by their average abundance, the $T_{11} < 220$ K and $T_{11} < 260$ K cloud fractions track each other closely in the near-equatorial area.

For the more tropically constrained domains the negative slopes for both the $T_{11} < 260$ K and $T_{11} < 220$ K regression lines shown in Table 1 result from simple expansion and contraction of the tropical cloud cover poleward and eastward under the influence of meteorological variations. It is well known, for example, that tropical convection alternately expands and contracts in the west Pacific under the influence of the Madden–Julian oscillation and other subseasonal variability (Lau and Chan 1986; Knutson and Weickmann 1987; Hendon and Salby 1994; Maloney and Hartmann 1998). If a box in the west-to-central Pacific is chosen as a reference, as LCH have done, then one obtains a negative correlation trivially from the tendency of tropical convection to retreat to the regions of highest SST when dynamical conditions are unfavorable for convection.

Table 1. Linear regression results for various domains, critical 11-μm temperatures, and done with and without high-pass filtering. Slope is the regression coefficient, the cloud fraction change per degree of cloud-weighted SST; *R* is the correlation of the regression, and σ_{SST} is the standard deviation of the cloud-weighted SST in K.

$T_{11} < 260$ K	Unfiltered			High-pass filtered		
	Slope	R	σ_{SST}	Slope	R	σ_{SST}
30°S–30°N	–0.0215	–0.273	0.53	–0.0133	–0.224	0.52
25°S–25°N	–0.0475	–0.419	0.38	–0.0234	–0.245	0.34
20°S–20°N	–0.0505	–0.323	0.28	–0.0225	–0.163	0.25
15°S–15°N	–0.0386	–0.222	0.26	–0.0160	–0.097	0.23
$T_{11} < 220$ K	Unfiltered			High-pass filtered		
	Slope	R	σ_{SST}	Slope	R	σ_{SST}
30°S–30°N	–0.0032	–0.141	0.38	–0.0003	–0.008	0.35
25°S–25°N	–0.0090	–0.272	0.30	–0.0036	–0.128	0.29
20°S–20°N	–0.0080	–0.206	0.27	–0.0028	–0.082	0.27
15°S–15°N	–0.0030	–0.087	0.27	–0.0030	–0.086	0.26

Regression maps of $T_{11} < 260$ K cloud fraction and wind vectors on $T_{11} < 260$ K cloud-weighted SST in the domains restricted to 15°S–15°N (Fig. 6) and 20°S–20°N (not shown) show that increases in cloud-weighted SST result when convective cloud fraction decreases north of the equator in the central Pacific and increases near Indonesia in the region from the equator to 10°S. The strong relationship of cloud fraction in the region north of the equator in the central Pacific to cloud-weighted SST shown in Fig. 6 appears in that location because that is where the coolest SSTs in the 15°S–15°N domain are found. So the pattern in Fig. 6 is entirely analogous to that in Fig. 2 in the sense that it shows that the cloud-weighted SST statistic is driven by cloud variations over the coldest water, and this leads trivially to a negative correlation between cloud-weighted SST and cloud fraction. If the same analysis is done using the $T_{11} < 220$ K cloud fraction and cloud-weighted SST, regression patterns of cloud fraction and winds are obtained that are very similar to those for the case of $T_{11} < 260$ K shown in Fig. 6. This confirms that the highest convective clouds and the associated anvil clouds vary proportionally, and that the variations in cloud-weighted SST result from changes in the amount of convection over the cooler water in the domain. There is no evidence in this of any change in the ratio of anvil area to convective area.

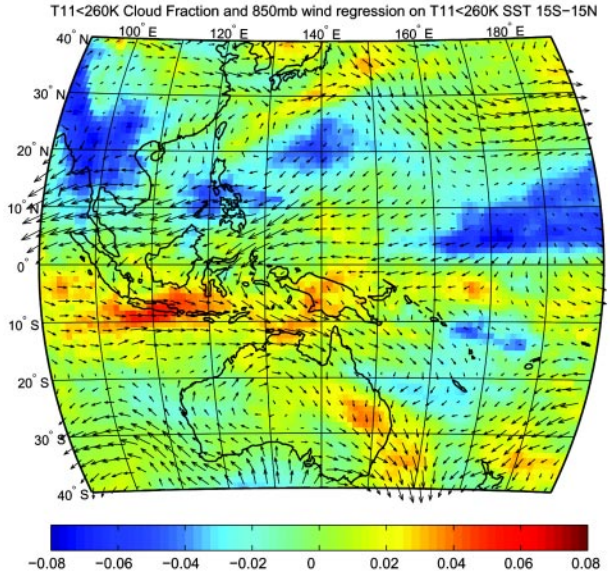

Fig. 6. Regression of the T_{11}<260 K cloud cover and the 850-mb wind vectors onto the T_{11}<260 K cloud-weighted SST for the region 15°S–15°N, 130°E–170°W using the high-pass-filtered cloud-weighted SST as in Fig. 2. The largest wind vectors shown have a magnitude of about 10 m s^{-1}.

CONCLUSIONS. We have presented an analysis of the spatial patterns of anomalous cloudiness and winds that are associated with the correlations between cloud fraction and cloud-weighted SST discussed in LCH. The variations in cloud-weighted SST for the domain that LCH used are associated with shifting patterns of cloudiness in the subtropics associated with extratropical wind anomalies. The variations of $T_{11} < 260$ K cloudiness that influence the cloud-weighted SST are more than 1000 km removed from deep convective cores with $T_{11} < 220$ K. It is unreasonable to interpret these changes as evidence that deep tropical convective anvils contract in response to SST increases. Moreover, the nature of the cloud-weighted SST statistic is such that any variation in cloud fraction over the coldest water must produce a negative correlation with cloud fraction, a fact that has no useful interpretation in climate sensitivity analysis. Therefore, the observational analysis in LCH lends no support to the hypothesis that increased SST decreases the area covered by tropical anvil cloud.

ACKNOWLEDGMENTS. This work was supported by NASA EOS Interdisciplinary Science investigation under Grant NAGS5-10624. Dr. Ming-Dah Chou made the cloud data conveniently available to us. M. B. Baker, Q. Fu, H. Harrison, and C. B. Leovy provided useful suggestions during the development of this paper.

REFERENCES

Hendon, H. H., and M. L. Salby, 1994: The life cycle of the Madden–Julian oscillation. *J. Atmos. Sci.,* **51,** 2225–2237.

Hoskins, B. J., and D. F. Karoly, 1981: The steady linear response of a spherical atmosphere to thermal and orographic forcing. *J. Atmos. Sci.,* **38,** 1179–1196.

Knutson, T. R., and K. M. Weickmann, 1987: 30–60 day atmospheric oscillations: Composite life cycles of convection and circulation anomalies. *Mon. Wea. Rev.,* **115,** 1407–1436.

Lau, K.-M., and P. H. Chan, 1986: Aspects of the 40–50 day oscillation during northern summer as inferred from outgoing longwave radiation. *Mon. Wea. Rev.,* **114,** 1354–1367.

Leith, C. E., 1973: The standard error of time-averaged estimates of climatic means. *J. Appl. Meteor.,* **12,** 1066–1069.

Lindzen, R. S., M. D. Chou, and A. Y. Hou, 2001: Does the earth have an adaptive infrared iris? *Bull. Amer. Meteor. Soc.,* **82,** 417–432.

Maloney, E. D., and D. L. Hartmann, 1998: Frictional moisture convergence in a composite life cycle of the Madden–Julian oscillation. *J. Climate,* **11,** 2387–2403.